JEFFREY H. SMART

SEASONAL AND SPATIAL VARIATIONS IN THE ATTENUATION OF LIGHT IN THE NORTH ATLANTIC OCEAN

This article examines seasonal and spatial variations in the average depth profiles of the diffuse attenuation coefficient, K_d, for visible light propagating downward from the ocean surface at wavelengths of 490 and 532 nm. Profiles of the depth of the nth attenuation length are also shown. Spring, summer, and fall data from the northwestern and north central Atlantic Ocean and winter data from the northeastern Atlantic Ocean are studied. Variations in the depth-integrated K_d profiles are important because they are related to the depth penetration achievable by an airborne active optical antisubmarine warfare system.

INTRODUCTION

Numerous investigators have tried to characterize the diffuse attenuation coefficient (hereafter denoted as K_d) for various ocean areas and for the different seasons. Platt and Sathyendranath[1] generated numerical fits to averaged profiles from coastal and open-ocean regions, and they divided the North Atlantic into provinces that extended from North America to Europe and over large ranges in latitude (e.g., from $10.0°$ to $37.0°$N and from $37.0°$ to $50.0°$N). In addition, numerous papers have attempted to model chlorophyll concentrations (which are closely correlated with K_d) using data on available sunlight as a function of latitude and season, nutrient concentrations, and mixed-layer depths (see, for example, Refs. 2–4). The main problems with using the outputs from the various empirical fits and models are that (1) they average very large geographic areas, often masking significant variations that occur near features such as the Gulf Stream, (2) the empirical fits sometimes ignore seasonal changes (e.g., Platt and Sathyendranath[1]), and (3) the depth extent of the models is insufficient for some applications. To avoid these problems, the data analyzed in this article have spatial averaging of a few degrees, at most, in latitude and longitude, monthly averages are used to avoid temporal aliasing, and the profiles extend down to at least 100 m.

This article describes the average depth profile of K_d and the depth of the nth attenuation length, where

$$\text{number of attenuation lengths} = \int_0^z K_d \, dz. \quad (1)$$

Downwelling light (light propagating downward) decays as $e^{-K_d z}$. The value of K_d depends on the wavelength of the light and on the depth of the water column because of variations in the particulates and dissolved substances. The depth of one attenuation length is the depth z at which light has decreased to e^{-1} of its surface value, and the depth of the nth attenuation length is the depth at which light has decreased to e^{-n} of its surface value. In this article, profiles of K_d are provided at 490 and 532 nm for

the geographic areas and seasons indicated in Table 1 and Figure 1. Despite the incomplete spatial and temporal coverage across the North Atlantic Ocean, this article should serve as a useful resource to estimate the optical characteristics in the areas studied.

The purpose of this article is to characterize the seasonal and spatial variations in diffuse attenuation at 490 and 532 nm. Because K_d frequently changes with depth, profiles of depth versus number of attenuation lengths are required to characterize the attenuation of light as it propagates from the surface downward into the water column. Large K_d values imply a low optical penetration range, and the depth of the nth attenuation length will be relatively shallow. Small K_d values imply a deep penetration range, and the depth of the nth attenuation length will be correspondingly deeper. The dependence of K_d on wavelength is related to the wavelength dependence of an airborne active optical antisubmarine warfare (ASW) system. For example, in waters where K_d at 532 nm is double that at 490 nm, an ASW system operating at 532 nm will generally have a significantly decreased depth range compared with an identical system operating at

Table 1. Summary of geographic and seasonal coverage of data discussed in this article.

Region	Latitude (°N)	Longitude (°W)	Season[a]
North Atlantic[b]	30.0–44.5	27.0–65.5	Spring
	30.0–50.0	50.0–60.0	Summer
	10.0–40.0	60.0–79.0	Fall
North Atlantic[c]	28.0–37.0	14.5–32.5	Winter

[a]Spring: 1 Apr–15 Jun; summer: 16 Jun–15 Sep; fall: 16 Sep–20 Dec; winter: 21 Dec–31 Mar. Periods associated with each season have been chosen to roughly match the known changes that occur in the mixed layer depth and related onset of the spring bloom.
[b]Bedford Institute of Oceanography chlorophyll data were provided by T. Platt (pers. comm., 17 Mar 1992).
[c]Naval Oceanographic Office irradiance-derived K_d profiles and chlorophyll data purchased from the National Ocean Data Center.
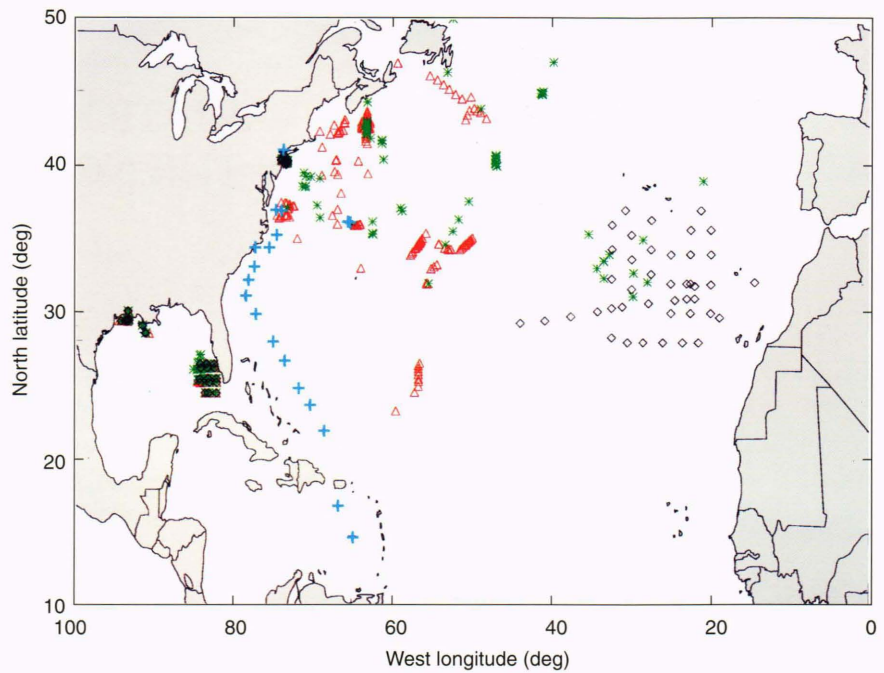
Figure 1. Data locations and corresponding seasons. Black: winter; green: spring; red: summer; blue: fall.

490 nm. The depth range of such systems actually depends on several elements, including the backscatter coefficient $\beta(\pi)$, which is likely to decrease with wavelength, leading to a higher target contrast and signal-to-noise ratio (SNR). When K_d increases with wavelength, however, SNR decreases. A detailed discussion of these competing effects is beyond the scope of this article.

An active optical system, such as a lidar, has its penetration depth specified as a number of attenuation lengths. The attenuation length profiles provided here allow one to relate this number to a physical depth in meters. Such a relationship is very useful to a submarine trying to operate at a depth below the range of known lidar systems.

DATA TYPES AND PROCESSING ASSUMPTIONS

The primary types of data presented here are chlorophyll-a concentration profiles (chlorophyll-a is the most prevalent form of chlorophyll) and K_d profiles derived from irradiance profiles. These data types, along with their potential errors, are discussed in the following paragraphs.

Chlorophyll-Derived K_d Profiles

The most common measure of the biomass in the ocean is the chlorophyll-a concentration. The total concentration C of chlorophyll-a and its decay products (known as phaeophytin) is closely correlated with K_d at 490 nm.[5-7] The Gordon-Morel regression relationship given by

$$K_d \text{ at 490 nm (m}^{-1}) = 0.0217 + 0.069C^{0.702} \quad (2)$$

where C is in milligrams per cubic meter,[5] is used to convert C to K_d at 490 nm. For Equation 2, the coefficient of determination $r^2 = 0.95$, and the number of samples is

$N = 121$. This regression is based on open-ocean (Jerlov Type I) waters and is appropriate to use over the total pigment concentration range of 0.02 to 40 mg/m³. The algorithm produces K_d profiles generally consistent within 20% of irradiance-derived K_d profiles, and averaging many such profiles can further reduce the discrepancy. As described later, irradiance-derived profiles provide a direct measure of the diffuse attenuation coefficient; therefore, they are often used as a standard by which one can assess the accuracy of other measures of K_d.

A potentially serious source of error occurs when Equation 2 is applied to concentrations of chlorophyll-a alone, that is, when the phaeophytin concentration is not included, because the regression specified in Equation 2 assumes that C includes both. For example, Figure 2A shows the difference between the total concentration of chlorophyll-a plus phaeophytin and that of only chlorophyll-a. In the figure, the error increases with increasing depth because the depth of the maximum phaeophytin concentration is generally deeper than that of the chlorophyll-a. In this article, the North Atlantic Ocean concentration data do not usually include phaeophytin. Using Gulf of Alaska profiles that contained both chlorophyll-a and phaeophytin concentrations, Stark[9] showed that neglecting the phaeophytin concentration led to fractional errors in K_d of up to 38% with an average error of 8.5%. He did not see any depth dependence of the errors, however. Stark used an effective K defined as the integral of K_d from the surface to a depth z. He computed K_d at 490 nm from C using the Smith–Baker algorithm[7] $K(490) = 0.0212 + 0.121C\exp[-(0.963)^2(\log_{10}2C)^2] + 0.001C^2$.

As indicated in Figure 2B, the average K_d computed without including phaeophytin is 20% less than K_d computed when phaeophytin is included. Therefore, depths of attenuation length computed without including phaeophytin will be about 20% too deep for these particular
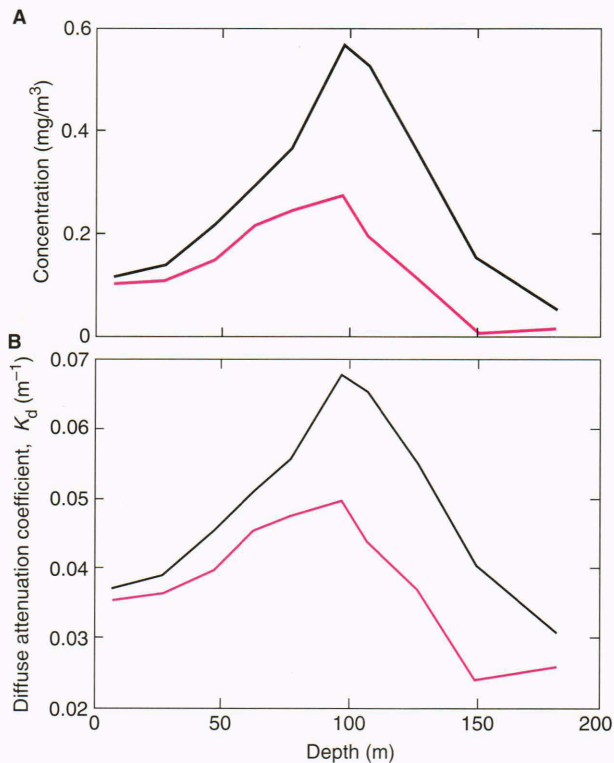
Figure 2. Examples of pigment concentration and diffuse attenuation coefficient (K_d) profiles computed with and without the contribution from phaeophytin. Black curves: chlorophyll-a + phaeophytin; red curves: chlorophyll-a. **A.** Pigment concentration profiles; average difference = 47%, maximum difference = 94%. **B.** K_d profiles; average difference = 20%, maximum difference = 40%. The data shown come from the Hawaiian Ocean Time Series Station Alpha at 22.75°N, 158.00°W in January 1990.[8]

data. The error is less than 20% in the near-surface waters where the discrepancy is least. Morel and Berthon[10] conducted a thorough study of the ratio ρ = (concentration of chlorophyll-a)/(concentration of chlorophyll-a + phaeophytin) using about 1400 profiles from around the world. When averaged from the surface to the euphotic depth, they found ρ to be about 0.65 in oligotrophic waters such as the Sargasso Sea and about 0.80 in eutrophic waters such as the Gulf of Alaska, and the ρ profiles decreased with increasing depth. (The euphotic depth is defined as the depth above which the net rate of photosynthesis is positive, that is, chlorophyll growth occurs. This depth is nominally where the light has decreased to 1% of its surface value. Oligotrophic waters are defined as waters suffering from nutrient depletion and hence sustaining relatively low concentrations of chlorophyll. Eutrophic waters are defined as waters having a plentiful supply of nutrients and hence sustaining relatively high concentrations of chlorophyll.) When these effects are propagated through Equation 2, we find that failures to include phaeophytin will lead to K_d values that are low by about 16% in oligotrophic waters and by about 13% in eutrophic waters. This calculation was performed using $C = 0.15$ μg/L for oligotrophic waters, corresponding to $K_d = 0.04$/m, and $C = 1.2$ μg/L for eutrophic waters, corresponding to $K_d = 0.10$/m, and as-

suming that the true value of C should be $C/0.65$ and $C/0.8$, respectively.

Irradiance K_d Profiles

The second way to measure the attenuation of light is by using K_d profiles obtained by lowering a spectral radiometer into the water and measuring the slope of the downwelling irradiance profile, $E_d(\lambda, z)$, where the wavelength λ generally spans the visible spectrum. Specifically,

$$K_d(\lambda, z) = -1/E_d \, dE_d/dz. \qquad (3)$$

These K_d profiles are subject to spurious variations in E_d caused by surface wave focusing, passage of clouds, ship shadow, and instrument tilt. They may also be affected by the Sun's elevation. No attempt was made to correct the data for the zenith angle of the Sun, because the variability induced by the other elements is probably greater than that caused by the Sun's zenith angle. Baker and Smith[11] showed that in turbid waters the Sun's zenith angle introduces a maximum change in K_d at 490 nm of less than 5%. In less turbid waters, however, Kirk[12] indicated that the error could be several times as great. Overall, individual K_d profiles are probably accurate to about 15%, and because the errors are generally random, averaging several profiles together further improves the results.

Once the K_d profiles are obtained at any given wavelength (usually at 490 nm), they can be converted to other wavelengths by using the Austin–Petzold model.[13] This model uses the following equation for the conversion from 490 to 532 nm:

$$K_d \text{ at 532 nm} = (0.68052/1.0)$$
$$\times [(K_d \text{ at 490 nm}) - 0.0224] + 0.05362. \qquad (4)$$

The model was generated by using data from seventy-six stations obtained between 1967 and 1979 in a wide range of coastal and open-ocean environments, such as the Gulf of Mexico, the Sea of Japan, the Sargasso Sea, and the equatorial Pacific. The majority of the profiles had a maximum depth of 30 m or less, so the analysis was later redone[14] using data from eighty-three stations obtained from 1985 to 1987 to a depth of 200 m and ranging from 24.4° to 77.4°N. The later analysis showed that the original model had the following coefficients of variation as a function of wavelength λ:

$$\frac{K_d \text{ (model)}}{K_d \text{ (measured)}} \quad < 8\% \text{ for } \lambda < 590 \text{ nm}$$

(11% at 410 nm and 4–5% for 530–548 nm)

$$\frac{K_d \text{ (model)}}{K_d \text{ (measured)}} \quad \geq 9\% \text{ for } \lambda > 590 \text{ nm}$$

(31% at 670 nm)

The model is less accurate at wavelengths greater than 590 nm because Raman scattering introduces light at these wavelengths that was originally at a lower wave-

length. For more details about Raman scattering, see the boxed insert on the next page.

To avoid instrument noise problems and excessive Raman effects, Austin and Petzold's model[13] is based solely on K_d values averaged from the surface to the depth where the light is reduced to 10% of its surface value. For water having K_d at 490 nm = 0.067/m, the 10% depth is reached at about 34 m, but at 630 nm, this depth is reached by about 7 m, and at 695 nm, by about 4 m. Therefore, their model is actually comparing K_d values from different depth ranges, and the model is based on relatively shallow data. Nevertheless, because of Raman contamination at 532 nm (described in the boxed insert), it is generally more accurate to compute K_d at 532 nm from K_d at 490 nm by using the Austin–Petzold model[13] than it is to compute K_d at 532 nm directly from E_d profiles at 532 nm.

To summarize, the results presented in this article are subject to the following data caveats:

1. K_d profiles obtained from pigment concentrations are accurate to about 20% if both chlorophyll-a and phaeophytin concentrations are provided. If only chlorophyll concentrations are used, however, then additional errors of about 13–16% are expected for eutrophic and oligotrophic waters, respectively. Figure 2 shows an example of how the error can depend on depth.

2. Profiles of K_d at 490 nm obtained from irradiance measurements are generally accurate to about 15%. K_d profiles derived from irradiance measurements at 490 nm can be converted to K_d profiles at 532 nm by using Equation 4, which is based on the Austin–Petzold model.[13]

3. The Austin–Petzold model[13] relates diffuse attenuation at one wavelength to that at another. The model is based on empirical fits, or regressions, among irradiance-based K_d profiles at various wavelengths using near-surface data. At 532 nm, the fit has a 4–5% coefficient of variation.

Besides these caveats on data accuracy, we assume that the user is interested in depth-averaged attenuation of light. The attenuation length profiles presented here are not generally appropriate for users who are interested in underwater vision, which often involves looking horizontally through the water.

SEASONAL AND SPATIAL VARIATIONS IN THE NORTH ATLANTIC OCEAN

We will now describe the results of our analysis for various seasons and regions in the North Atlantic Ocean. In each of the summary descriptions, the original individual chlorophyll- and irradiance-derived K_d profiles were examined to determine reasonable spatial and temporal averaging intervals such that the average K_d profiles would be representative of the original profiles. To indicate accuracy of the results, the standard deviations of the mean K_d profiles are shown, along with the number of independent samples from each location. The variability about the mean is generally caused by random measurement errors, so that the errors in the optical attenuation length profiles, which come from integrating the K_d profiles, are much smaller than what one calculates by as-

suming a systematic error equal to the standard deviations in K_d. That assumption does, however, provide an upper bound to the depth errors in the optical attenuation length profiles. By that assumption, the depth error is approximately $z\Delta K_d/K_d$, where z is the measured depth of the nth optical attenuation length and ΔK_d is the standard deviation in the measured K_d value. For example, for K_d = 0.05/m and z = 60 m (the depth of three attenuation lengths), a systematic (worst case) error of ΔK_d = 0.005/m results in an error in z of 9 m.

Winter Conditions of the Northeast Atlantic Ocean

As indicated in Table 1, the only comprehensive winter data for the North Atlantic Ocean came from the Naval Oceanographic Office profiles of K_d at 490 nm, obtained in the northeast Atlantic Ocean using E_d data. Figure 3A shows a map of the mean profile locations, and Figure 3B shows the corresponding mean K_d profiles. The overall dimensions of the map approximate the spatial range of the original data. Among the mean profiles, the surface K_d values increase noticeably as a function of latitude (compare the 28.0°–30.0°N and the 35.0°–37.0°N mean profiles). Also, in the range of 35.0°–37.0°N, a longitudinal difference occurs between the mean profile from 20.0°–22.5°W and that from 27.5°–32.5°W. Below 100 m, however, the profiles tend to converge. Figure 3C shows the corresponding attenuation length profiles computed from the K_d data. A significant gradient occurs in the K_d profiles below about 100 m, but because it occurs so deep, it introduces little curvature to the attenuation length profiles.

The profiles of K_d at 490 nm were converted to profiles of K_d at 532 nm by using Equation 4, and they are shown, along with the corresponding 532-nm attenuation length profiles, in Figure 4. As indicated in Equation 4, the conversion from 490 to 532 nm amounts to (1) removing the pure water contribution from K_d at 490 nm, (2) applying a scale factor, and (3) adding an offset (equal to the pure seawater value of K_d at 532 nm). In general, the net effect is to significantly decrease depths of attenuation lengths, primarily because the pure water value of K_d at 532 nm is greater than that at 490 nm, and to decrease the spread in attenuation length profiles. A comparison of Figures 3C and 4B illustrates these effects. For example, at 490 nm, the depth of four attenuation lengths ranges from about 78 to 103 m, whereas at 532 nm, it ranges from about 54 to 62 m. Table 2 lists the depths of 0.5 to 6.5 attenuation lengths at 0.5 intervals at each wavelength.

As shown in Ref. 15, the depths of one attenuation length agree fairly well (within 28%) with corresponding spatial averages of coastal zone color scanner (CZCS) satellite data. This result suggests that we could use CZCS data to estimate depths of one attenuation length for other longitudinal ranges across the North Atlantic during winter months to fill in the vast area left unsampled by the available *in situ* data. The CZCS data, which were collected by NASA between 1978 and 1986, cover nearly the entire world. Although the raw data are subject to large errors, when Stark[16] used 20 × 20 km CZCS averages for

EFFECT OF RAMAN SCATTERING ON K_d PROFILES

An inherent assumption in using Equation 3 [$K_d(\lambda, z) = -1/E_d \, dE_d/dz$] as a measure of the absorption of downwelling irradiance E_d is that the only source of $E_d(\lambda)$ is that present at the ocean surface. (The absorption coefficient a and the diffuse attenuation coefficient K_d are frequently used interchangeably, although a is actually an inherent optical property and K_d is an apparent optical property that, excluding Raman effects, is approximately $a + b_b$, where b_b is scattering in the backward hemisphere. Generally, $b_b \ll a$, so $K_d \approx a$.) This assumption is violated, however, because a fraction of the light absorbed by water molecules at λ_1 is known to be re-emitted at λ_2. This emission is known as the Raman effect and is described further in Refs. 19 and 20. At $\lambda \approx 680$ nm (i.e., considerably higher than the wavelengths of interest in this article), particulates and dissolved substances within the water column exhibit a similar phenomenon known as fluorescence.[21] Fluorescence dominates the Raman effect at these wavelengths.

This discussion summarizes to what extent the Raman effect distorts the measured $K_d(\lambda)$ profiles and shows that in relatively clear water the effect is negligible at 490 nm but significant at 532 nm for depths greater than or equal to 20 m. The Sun produces a broad spectrum of E_d, and ocean water absorbs this light at rates that differ as a function of λ; the minimum absorption occurs near 490 nm for the clearest ocean waters. The minimum is actually at about 450 nm in perfectly pure seawater, but the presence of even small amounts of impurities, such as chlorophyll, moves the minimum toward about 490 nm. Refer to Figure 4 in Ref. 13 to see how the minimum shifts as K_d at 490 nm increases.
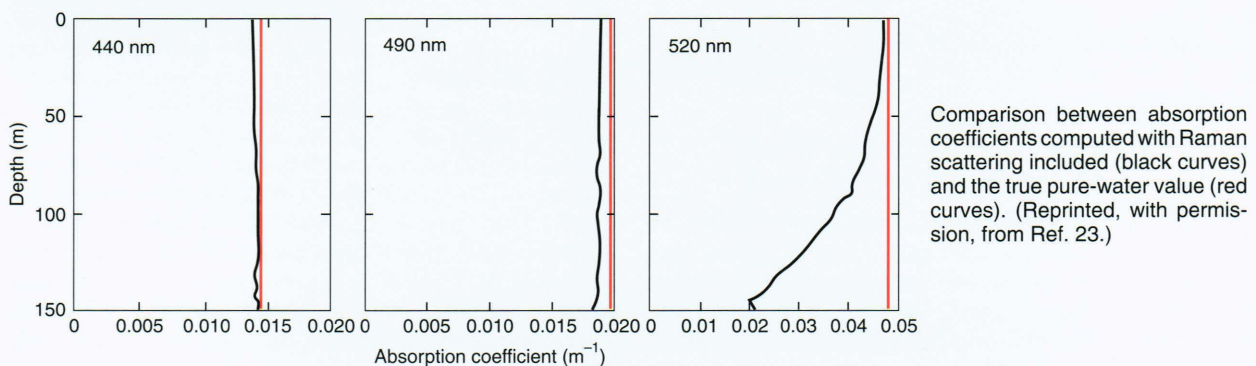
Stavn and Weidemann[22,23] have studied the Raman effect extensively using Monte Carlo simulations for pure water, and their results at 440, 490, and 520 nm are shown in the accompanying figure. At 440 nm, the Raman effect leads to an absorption profile slightly lower than the true absorption (a_w) of the water itself. The bias decreases as depth increases because the source of the Raman emission is at 383 nm, and at that wavelength, a_w is significantly higher than at 440 nm. Therefore, the source of the Raman irradiance decreases at a faster rate than does the downwelling surface light present at the emission wavelength. The equation that gives the Raman emission is $(1/\lambda_{in}) - 3357$ cm^{-1} = $(1/\lambda_{out})$, where λ is in centimeters.

The figure shows that at 490 nm, the Raman effect produces a bias of less than -0.001 m^{-1}, which is negligible

in comparison with our measured K_d values of 0.03 m^{-1} or greater. The effect is nearly depth-independent because the source wavelength, $\lambda = 421$ nm, has an absorption value only slightly different from that at 490 nm. At 520 nm, however, the bias increases greatly with depth, because the absorption at the source wavelength (443 nm) is much less than at 520 nm. The bias produces an error in absorption that exceeds 100% at depths greater than 100 m. The effect becomes even more severe at higher wavelengths[23] because the difference between absorption at the source and emissions grows.

Stavn and Weidemann's results[22,23] are for pure ocean water, devoid of chlorophyll. The addition of chlorophyll increases absorption, and therefore the relative effect of the Raman bias should decrease proportionately. Also, the chlorophyll tends to decrease the difference between source and emission absorption, thereby decreasing the depth dependence of the Raman bias. For the most extreme condition, when the chlorophyll concentration is very high, the absorption at the source wavelength will be so great that it obviates the concern about the Raman effect because the light will have exceeded six attenuation lengths by a depth of 20 m. Despite these mitigations, Raman scattering is still a source of serious contamination, especially in relatively clear open-ocean waters. For example, Siegel and Dickey[24] measured open-ocean $K_d(\lambda)$, and at wavelengths of about 520 nm or greater, they obtained values lower than the theoretical value for pure water, clearly indicating the Raman bias.

In generating their empirical model that relates $K_d(\lambda_1)$ to $K_d(\lambda_2)$, Austin and Petzold[13] were aware of the danger of Raman bias, so they ensured that the effect would be minimal by restricting their regression to depths above the 10% light level (i.e., the depth where surface light has decreased by 90%). For example, for water having K_d at 520 nm = 0.067, the 10% depth is reached at 34 m. As shown in the figure, the error in absorption is relatively small above this depth even for pure water, and as discussed earlier, the error should be even less with the chlorophyll present. The point of this discussion is that by using the Austin–Petzold model[13] to compute profiles of K_d at 532 nm from profiles of K_d at 490 nm (which suffer from only a negligible Raman bias), rather than by using measured downwelling irradiance profiles at 532 nm, we have provided K_d and attenuation length profiles that are unlikely to be contaminated by any significant Raman effects.
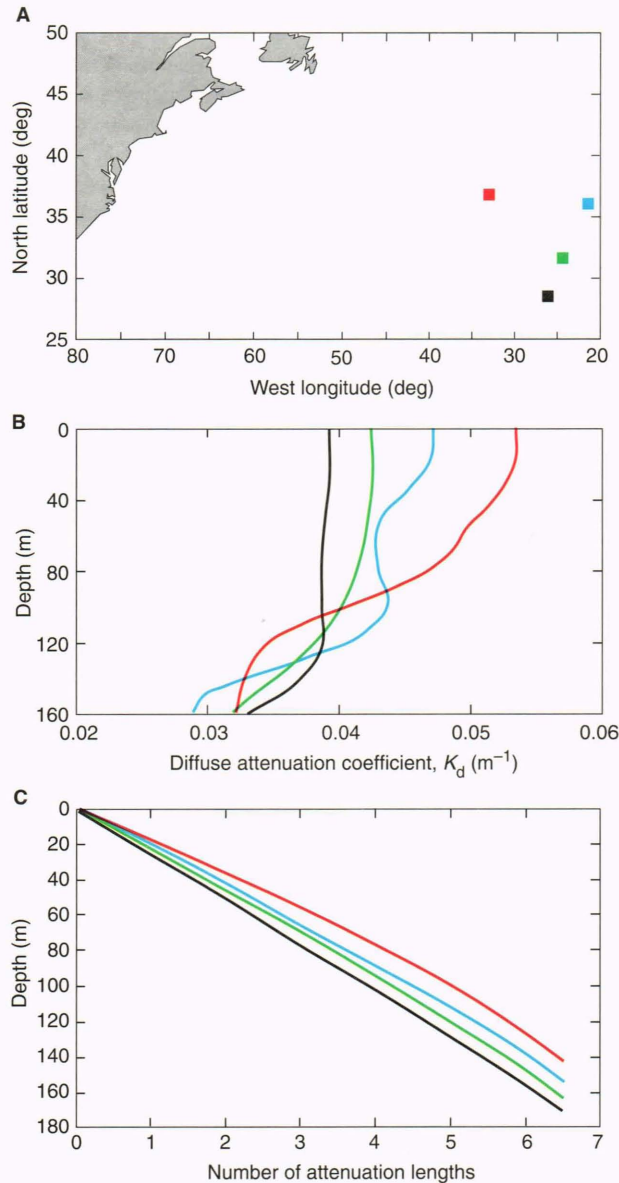

Comparison between absorption coefficients computed with Raman scattering included (black curves) and the true pure-water value (red curves). (Reprinted, with permission, from Ref. 23.)

A

B

A

B

Figure 4. Average winter 532-nm profiles of the diffuse attenuation coefficient (K_d) and attenuation length in the North Atlantic. Note the change in depth scale relative to the 490-nm profiles shown in Figure 3. **A.** Mean K_d profiles. **B.** Corresponding attenuation length profiles. Colors correspond to the same latitude and longitude locations given in Figure 3.

C

Figure 3. Average winter 490-nm profiles of the diffuse attenuation coefficient (K_d) and attenuation length. **A.** Mean profile locations. **B.** Mean K_d profiles. **C.** Corresponding attenuation length profiles. Black: 28.0°–30.0°N, 19.0°–32.5°W (17 profiles $\sigma = 0.003$/m); green: 30.0°–35.0°N, 14.5°–32.5°W (30 profiles, $\sigma = 0.004$/m); blue: 35.0°–37.0°N, 20.0°–22.5°W (6 profiles, $\sigma = 0.005$/m); red: 35.0°–37.0°N, 27.5°–32.5°W (7 profiles, $\sigma = 0.006$/m).

each month of the year, his results provided useful K_d estimates for vast ocean regions where *in situ* data are unavailable.

Spring, Summer, and Fall Conditions of the Northwest and North Central Atlantic Ocean

The preceding analysis described the most complete *in situ* data set available for obtaining winter K_d profiles in the North Atlantic Ocean. We now summarize the data available for spring, summer, and fall. As indicated in Table 1, the chlorophyll data from the Bedford Institute
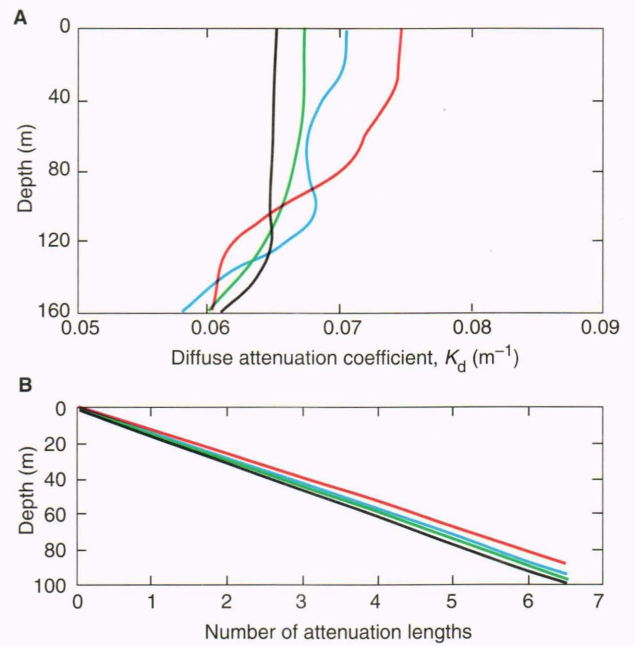
of Oceanography cover these seasons for portions of the Sargasso Sea and areas north of there. These areas are located in the northwest and north central Atlantic Ocean. The Sargasso Sea waters exhibit typical oligotrophic conditions; that is, they have low chlorophyll concentrations and, hence, low K_d values in the surface waters because of nutrient depletion, and they have subsurface maxima of varying amplitude at deeper depths. The waters north of the Sargasso Sea—near the Gulf Stream and just north of it—generally exhibit eutrophic conditions; that is, they have relatively high chlorophyll concentrations and, hence, high K_d values in the surface waters and substantially decreased values below a depth of about 50 m. A few profiles fit neither category because they are from a transition zone between the two.

The various conditions are shown in the mean spring K_d profiles, derived from the Bedford chlorophyll data, in Figure 5. The profiles from the north central Atlantic (30.0°–38.0°N, 27.0°–59.0°W; black and green curves) are typical of the oligotrophic Sargasso Sea waters, and the profiles from the northwest Atlantic (35.0°–45.0°N, 40.0°–65.5°W; blue, red, pink, and brown curves) are typical of eutrophic conditions. A transitional example is found in the early June data (42.5°–44.5°N, 61.5°–65.5°W; purple curve), which has a low surface K_d value of about 0.045/m, a subsurface peak of about 0.08/m at a depth of 30 m, and then a sharp decrease below that depth. This same location had the highest surface K_d values in early May (brown curve). The difference suggests that the Gulf Stream may have been farther south in the year that the May data were acquired. (The May data come from 1977, and the June data come from

Table 2. Summary of depths of attenuation lengths (in meters) in the northeast Atlantic Ocean in the winter.

No. of attenuation lengths	Depths of attenuation lengths (m) at various latitude (longitude) locations			
	28.0°–30.0°N (14.5°–32.5°W)	30.0°–35.0°N (14.5°–32.5°W)	35.0°–37.0°N (20.0°–22.5°W)	35.0°–37.0°N (27.5°–32.5°W)
	Wavelength = 490 nm			
0.5	12.7	11.8	10.6	9.3
1.0	25.5	23.6	21.3	18.7
1.5	38.2	35.3	32.2	28.1
2.0	51.1	47.2	43.3	37.6
2.5	63.9	59.0	54.8	47.4
3.0	76.8	71.0	66.5	57.3
3.5	89.8	83.1	78.1	67.5
4.0	102.7	95.4	89.8	77.9
4.5	115.6	107.9	101.3	88.8
5.0	128.5	120.8	112.9	100.6
5.5	141.8	134.2	125.3	113.8
6.0	155.9	148.6	139.2	128.2
6.5	170.9	163.9	155.6	143.3
	Wavelength = 532 nm			
0.5	7.7	7.4	7.1	6.7
1.0	15.4	14.9	14.2	13.4
1.5	23.0	22.3	21.3	20.1
2.0	30.7	29.7	28.5	26.8
2.5	38.4	37.2	35.7	33.5
3.0	46.1	44.6	43.0	40.3
3.5	53.8	52.1	50.3	47.1
4.0	61.5	59.5	57.7	54.0
4.5	69.3	67.0	65.1	60.9
5.0	77.0	74.5	72.5	67.9
5.5	84.7	82.0	79.9	74.9
6.0	92.4	89.6	87.3	82.0
6.5	100.2	97.2	94.7	89.2

1978.) The fact that the lowest surface K_d values occur the farthest south and that the highest occur the farthest north is consistent with czcs data.[16]

Figure 6 shows a similar set of mean K_d profiles, spanning a somewhat different spatial area, derived from summer Bedford chlorophyll data. The profiles from 30.0°–40.0°N, 50.0°–65.0°W (black, green, blue, and red curves) all have typical oligotrophic Sargasso Sea conditions, whereas those from 42.5°–50.0°N, 50.0°–65.0°W (brown and purple curves) are more eutrophic, and the one at 40.0°–42.5°N, 50.0°–65.0°N (pink curve) is a transition zone profile. Both of the eutrophic profiles, however, show signs of nutrient depletion in the upper 20 m, and the peak values (0.08 to 0.10/m) are considerably lower than those obtained at similar locations in the spring (0.14 to 0.16/m). This result is expected because more nutrients are available in the spring because of the preceding period of deep winter mixing, which leads to the well-known "spring bloom" of chlorophyll[17,18] at these temperate latitudes.

The fall K_d profiles derived from Bedford chlorophyll data and their locations are shown in Figure 7. The locations differ from the spring and summer data: some data are from the tropics (10.0°–20.0°N), and other data are from farther west (60.0°–79.0°W compared with 27.0°–65.5°W and 50.0°–65.0°W for the spring and summer data, respectively). The tropical K_d profile is similar to the oligotrophic spring and summer Sargasso Sea profiles, except that its mean value (≈0.05/m) is somewhat higher. The fall Sargasso Sea profile from 20.0°–30.0°N is noticeably different from the spring and summer Sargasso Sea profiles, however. It has no significant structure in the upper 100 m, whereas the spring and summer profiles have a pronounced subsurface maximum. Nevertheless, the mean fall values are about 0.035/m, similar to the mean spring and summer values of 0.03 to 0.04/m. The difference in the shape probably comes from some combination of the season (continued nutrient depletion may tend to eliminate the subsurface maximum), the more westerly location, and the deeper mixing that occurs in the fall.

The fall profile from 30.0°–35.0°W, 74.0°–79.0°W in Figure 7 (blue curve) comes from a transition region between the oligotrophic conditions to the southeast and the eutrophic conditions to the north and west. The eutrophic profile from 35.0°–40.0°N, 70.0°–75.0°W (red
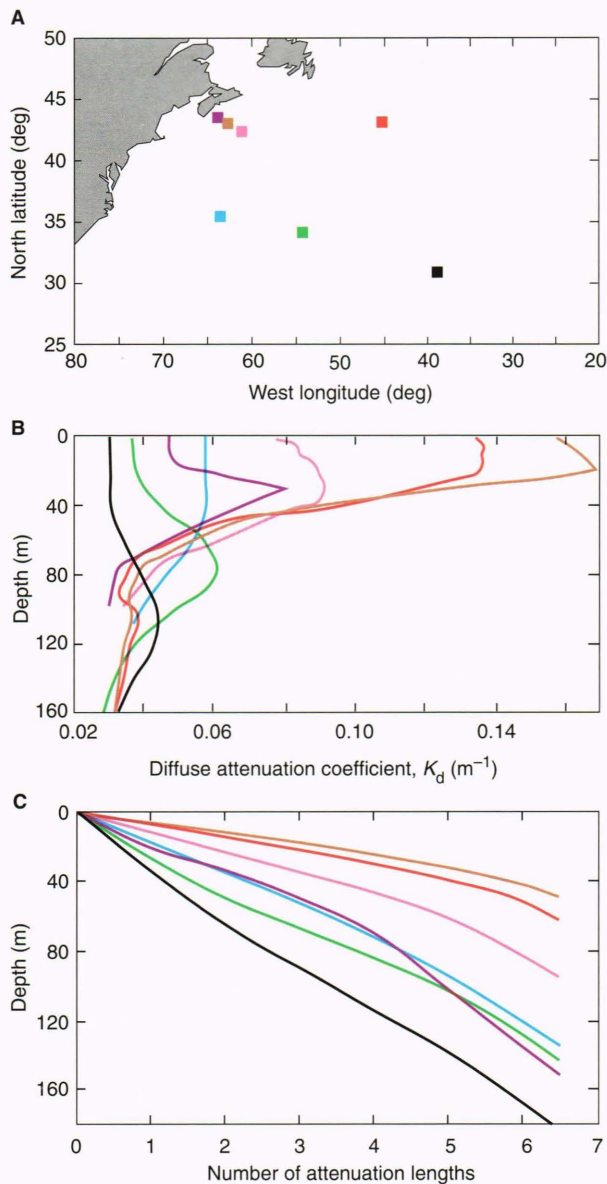
Figure 5. Average spring 490-nm profiles of the diffuse attenuation coefficient (K_d) and attenuation length. The two profiles from 42.5°N come from early May (brown) and early June (purple). **A.** Mean profile locations. **B.** Mean K_d profiles. **C.** Corresponding attenuation length profiles. Black: 30.0°–33.4°N, 27.0°–55.5°W (7 profiles, $\sigma = 0.002$/m); green: 33.5°–38.0°N, 28.0°–59.0°W (41 profiles, $\sigma = 0.008$/m); blue: 35.0°–35.5°N, 62.0°–63.0°W (27 profiles, $\sigma = 0.005$/m); red: 39.0°–45.0°N, 40.0°–50.0°W (18 profiles, $\sigma = 0.001$/m); pink: 40.0°–42.0°N, 60.0°–61.5°W (5 profiles, $\sigma = 0.010$/m); brown: 42.5°–44.5°N, 61.5°–65.5°W (17 profiles, $\sigma = 0.020$/m); purple: 42.5°–44.5°N, 61.5°–65.5°W (9 profiles, $\sigma = 0.010$/m).
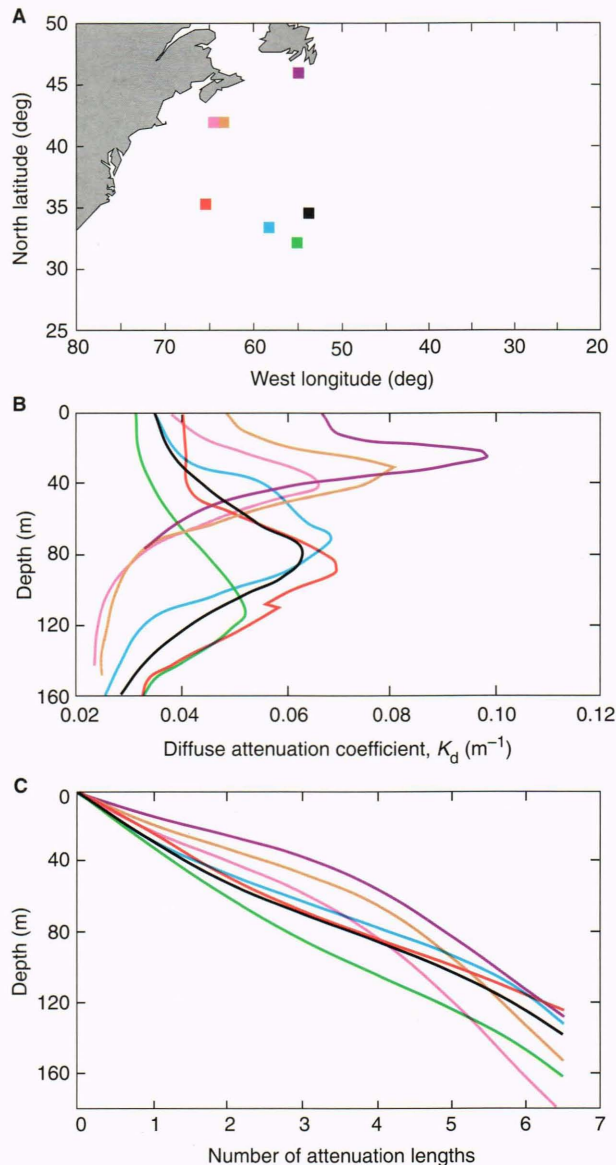
Figure 6. Average summer 490-nm profiles of the diffuse attenuation coefficient (K_d) and attenuation length. **A.** Mean profile locations. **B.** Mean K_d profiles. **C.** Corresponding attenuation length profiles. Black: 30.0°–35.0°N, 50.0°–55.0°W (36 profiles, $\sigma = 0.005$/m); green: 30.0°–32.5°N, 55.0°–65.0°W (11 profiles, $\sigma = 0.001$/m); blue: 32.5°–35.0°N, 55.0°–65.0°W (6 profiles, $\sigma = 0.010$/m); red: 35.0°–40.0°N, 50.0°–65.0°W (14 profiles, $\sigma = 0.004$/m); pink: 40.0°–42.5°N, 50.0°–65.0°W (17 profiles, $\sigma = 0.010$/m); brown: 42.5°–45.0°N, 50.0°–65.0°W (43 profiles, $\sigma = 0.010$/m); purple: 45.0°–50.0°N, 50.0°–60.0°W (5 profiles, $\sigma = 0.009$/m).

curve) represents an area that is in close proximity to the Gulf Stream and its associated eddies. The conditions there are expected to be more variable than in the areas farther south and east.

Figures 5C, 6C, and 7C show, respectively, the spring, summer, and fall mean 490-nm attenuation length profiles computed from the K_d profiles using Equation 1. Tables 3 to 5 contain the numerical values used to generate these figures. The largest range in K_d and depth of

attenuation lengths occurs in the spring, but all three profiles show substantial spatial variability. The differing regional coverage complicates direct season-to-season comparisons, but if the tropical climates are excluded, it appears that the spans of summer and fall depths of attenuation lengths are almost the same in the upper 100 m (i.e., down to four attenuation lengths). Also, the spring (30.0°–33.4°N, 27.0°–55.5°W) and summer (30.0°–32.5°N, 55.0°–65.0°W) Sargasso Sea attenuation

length profiles are very similar, and the spring (33.5°–38.0°N, 28.0°–59.0°W) and summer (30.0°–35.0°N, 50.0°–55.0°W) Sargasso Sea profiles are almost identical. The summer (30.0°–32.5°N, 55.0–65.0°W) and fall (20.0°–30.0°N, 68.0°–78.0°W) Sargasso Sea attenuation length profiles agree to within about 10 m.

Among the eutrophic profiles, however, larger differences occur. For example, the early May attenuation length profile (brown curve) shown in Figure 5C reaches four attenuation lengths at about 25 m, whereas in Figure 6C the summer profile from about the same region (brown curve) reaches that value at 65 m. As shown in Figure 7C, the fall profile from 35.0°–40.0°N, 70.0°–75.0°W (red curve) reaches four attenuation lengths at

about 40 m, but in Figure 6C, the summer profile from 35.0°–40.0°N, 50.0°–65.0°W (red curve) reaches that value at about 85 m.

The profiles shown in Figures 5 to 7 were converted from 490 to 532 nm using Equation 4, and the profiles at 532 nm are shown in Figures 8 to 10. The shape of the K_d profiles is unchanged by the wavelength conversion, but the range in values is diminished. The minimum values at 532 nm are about 0.06/m, compared with about 0.03/m at 490 nm. The effect on the attenuation length profiles is to decrease the depths at 532 nm relative to those at 490 nm, and this effect is greatest for the southern oligotrophic profiles. The attenuation length profiles are about the same at both wavelengths for the more northerly profiles. For example, compare the spring profiles from 42.5°–44.5°N, 61.5°–65.5°W (brown curves) in Figures 5 and 8.

SUMMARY

This article provides average depth profiles of the diffuse attenuation coefficient K_d at wavelengths of 490 and 532 nm for the locations shown in Figure 1. The data sources and spatial coverage are summarized in Table 1. The K_d profiles were then integrated to provide average profiles of the attenuation length, defined in Equation 1, at these same wavelengths. The attenuation length profiles characterize the seasonal and spatial variations in cumulative diffuse attenuation, computed from the surface downward, at the two wavelengths. For near-surface waters, we observe the following general characteristics.
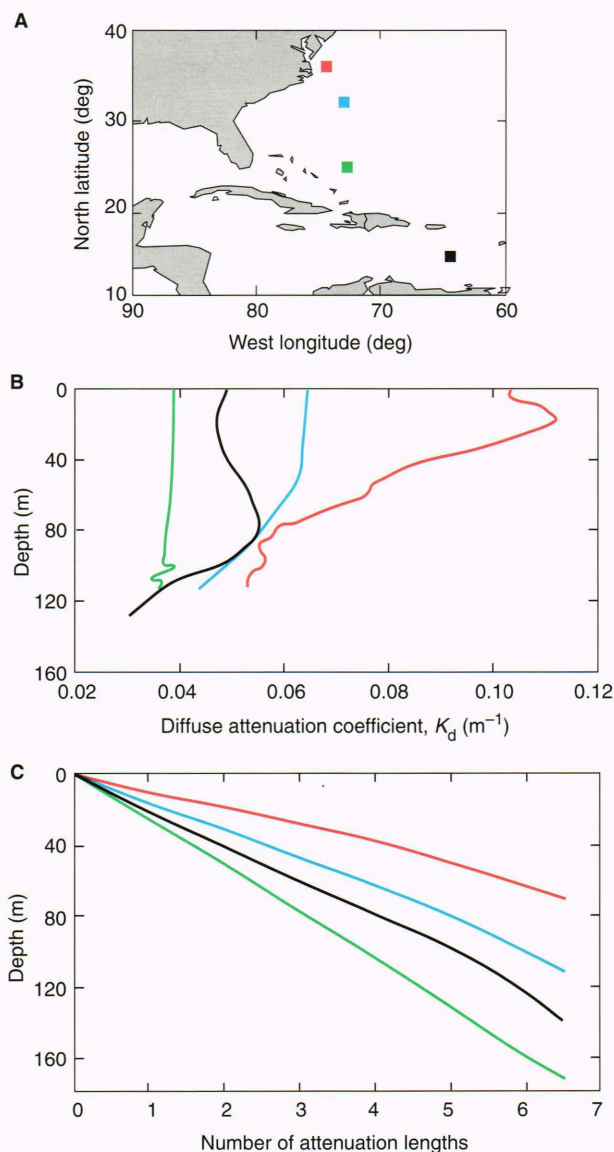

Figure 7. Average fall 490-nm profiles of the diffuse attenuation coefficient (K_d) and attenuation length. **A.** Mean profile locations. **B.** Mean K_d profiles. **C.** Corresponding attenuation length profiles. Black: 10.0°–20.0°N, 60.0°–65.0°W (15 profiles, $\sigma = 0.009$/m); green: 20.0°–30.0°N, 68.0°–78.0°W (5 profiles, $\sigma = 0.007$/m); blue: 30.0°–35.0°N, 74.0°–79.0°W (6 profiles, $\sigma = 0.008$/m); red: 35.0°–40.0°N, 70.0°–75.0°W (2 profiles, $\sigma = 0.013$/m).
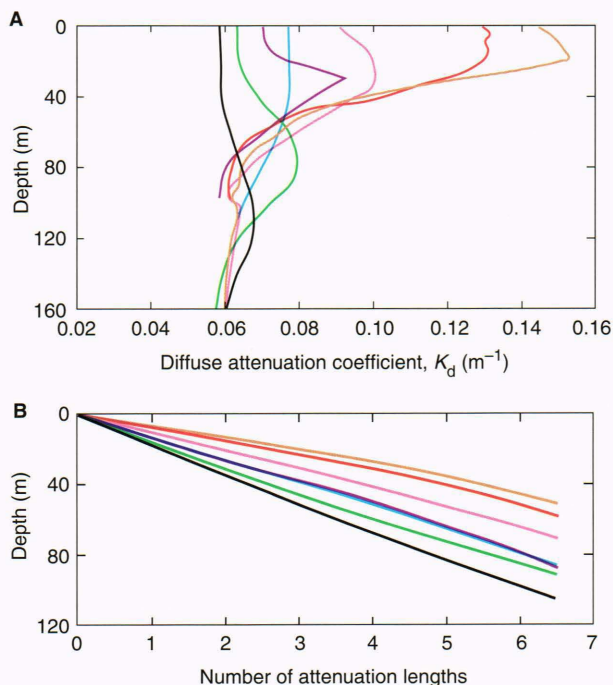

Figure 8. Average spring 532-nm profiles of the diffuse attenuation coefficient (K_d) and attenuation length in the North Atlantic. **A.** Mean K_d profiles. **B.** Corresponding attenuation length profiles. Colors correspond to the same latitude and longitude locations given in Figure 5.

Figure 9. Average summer 532-nm profiles of the diffuse attentuation coefficient (K_d) and attenuation length in the North Atlantic. **A.** Mean K_d profiles. **B.** Corresponding attenuation length profiles. Colors correspond to the same latitude and longitude locations given in Figure 6.

Figure 10. Average fall 532-nm profiles of the diffuse attenuation coefficient (K_d) and attenuation length in the North Atlantic. **A.** Mean K_d profiles. **B.** Corresponding attenuation length profiles. Colors correspond to the same latitude and longitude locations given in Figure 7.
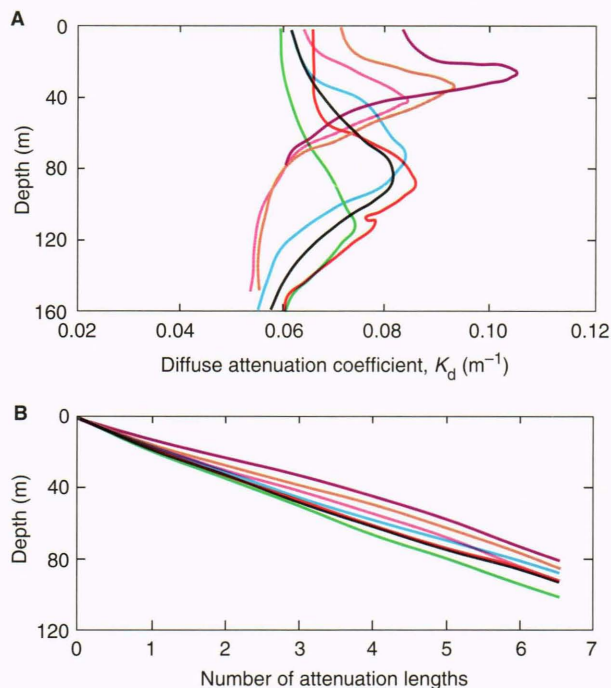
First, because K_d frequently changes with depth (as in Figs. 5 and 6), profiles of depth versus number of attenuation lengths are among the essential parameters required to characterize light propagation from the surface downward into the water column. If K_d were constant, as it nearly is in the northeast Atlantic Ocean winter data, then the attenuation profiles would be linear, and they would be characterized by a single number. Second, certain geographic areas consistently exhibit relatively high attenuation of light, whereas others exhibit low attenuation. For example, at both 490 and 532 nm, the northwest Atlantic Ocean north of the Gulf Stream has large K_d values (the depth of the first attenuation length is about 10 m or less). In contrast, areas with low K_d values at 490 nm include the northeast Atlantic Ocean (28.0°-37.0°N, 14.5°-32.5°W), the Sargasso Sea, and the tropics. In these areas the depth of the first attenuation length is about 20 m or greater. At 532 nm, however, the K_d values are intermediate (the depth of the first attenuation length is 10-20 m). Therefore, the depths of the attenuation lengths at 532 nm are shallower than at 490 nm by up to a factor of 2.

We find that the situation becomes more complicated when seasonal effects are considered. Relatively few profiles of K_d were available from the winter, and those come from the region 28.0°-37.0°N, 14.5°-32.5°W. For this region of the North Atlantic Ocean, as shown in Figures 3 and 4 and Table 2, the depths of attenuation lengths at 490 nm are 1.4 to 1.7 times deeper than at 532 nm. One attenuation length at 490 nm ranges from 19 to
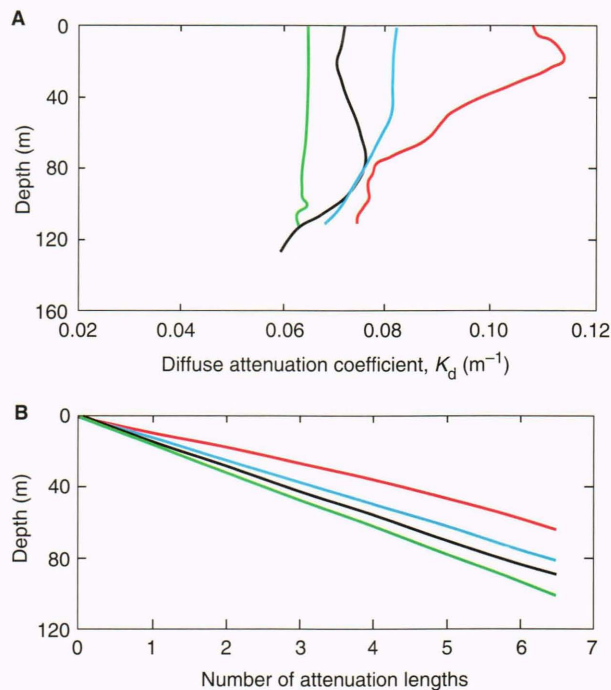
26 m; at 532 nm, the range is 13 to 15 m. At both 490 and 532 nm, diffuse attenuation decreases from north to south and from west to east. The depth of four attenuation lengths varies spatially among the locations by about 25 m or less at 490 nm, and by about 8 m or less at 532 nm.

More data were available from spring, summer, and fall, although the spatial coverage is not identical for all three seasons, and it does not overlap the winter locations. The spring data come from 30.0°-45.0°N, 27.0°-66.0°W and exhibit the following features: In the southern part of the region (30.0°-38.0°N, 27.0°-59.0°W), as shown in Figures 5 and 8 and Table 3, diffuse attenuation is very low at 490 nm; the depth of one attenuation length at 490 nm is about 27 to 33 m, which is up to 1.9 times deeper than at 532 nm. North of the Gulf Stream (40.0°-42.0°N, 60.0°-61.5°W), the attenuation increases significantly; the depth of one attenuation length is about 12 m or less, and the values are about the same at both wavelengths. Diffuse attenuation at both wavelengths generally decreases from north to south, but the spatial variations are complicated by the presence of the Gulf Stream. A very wide range in attenuation length profiles occurs across the area. For example, the depth of four attenuation lengths varies spatially up to 89 m at 490 nm and 40 m at 532 nm.

The summer data come from the region bounded by 30.0°-50.0°N, 50.0°-65.0°W. As shown in Figures 6 and 9 and Table 4, the diffuse attenuation at 490 nm is intermediate north of the Gulf Stream and low south of it. Also, the depth of one attenuation length at 490 nm

Table 3. Summary of depths of attenuation lengths (in meters) in the Sargasso Sea in the spring.

No. of attenuation lengths	Depths of attenuation lengths (m) at various latitude (longitude) locations						
	30.0°-33.4°N (27.0°-55.5°W)	33.5°-38.0°N (28.0°-59.0°W)	35.0°-35.5°N (62.0°-63.0°W)	39.0°-45.0°N (40.0°-50.0°W)	40.0°-42.0°N (60.0°-61.5°W)	42.5°-44.5°N (61.5°-65.5°W)	42.5°-44.5°N (61.5°-65.5°W)
			Wavelength = 490 nm				
0.5	16.7	13.6	8.8	3.7	6.3	3.2	10.7
1.0	33.2	26.8	17.6	7.4	12.2	6.3	20.3
1.5	49.4	38.8	26.3	11.1	17.9	9.4	27.9
2.0	64.4	49.5	35.1	14.8	23.5	12.4	34.4
2.5	78.0	59.0	43.8	18.4	29.0	15.4	41.6
3.0	90.5	67.7	52.8	22.2	34.5	18.4	49.7
3.5	102.3	76.0	62.0	26.0	40.2	21.4	59.0
4.0	113.7	84.4	71.9	30.1	46.5	24.7	70.6
4.5	125.4	93.2	82.5	34.4	53.4	28.2	85.9
5.0	138.3	103.2	94.5	39.2	61.2	32.3	102.3
5.5	152.3	114.7	107.6	44.7	70.5	36.9	119.1
6.0	167.5	128.5	121.3	52.2	82.1	42.4	135.9
6.5	182.8	143.9	135.0	62.1	95.4	49.2	152.7
			Wavelength = 532 nm				
0.5	8.5	7.9	6.5	3.8	5.4	3.4	7.1
1.0	17.0	15.8	13.0	7.7	10.7	6.8	14.2
1.5	25.5	23.6	19.4	11.5	15.8	10.2	20.8
2.0	34.0	31.2	25.9	15.3	20.9	13.5	26.8
2.5	42.4	38.7	32.4	19.1	25.9	16.8	32.4
3.0	50.8	45.9	38.9	23.0	30.8	20.1	38.0
3.5	59.0	52.8	45.3	27.0	35.9	23.5	44.1
4.0	67.1	59.5	51.9	31.1	41.0	27.1	50.3
4.5	75.0	65.9	58.5	35.5	46.4	31.1	57.0
5.0	82.7	72.3	65.3	40.1	52.1	35.4	64.1
5.5	90.3	78.6	72.1	45.2	58.1	40.2	71.7
6.0	97.7	84.9	79.2	51.1	64.4	45.6	79.9
6.5	105.1	91.4	86.5	57.7	71.2	51.5	88.3

ranges from 15 m in the northern part of the region (45.0°-50.0°N, 50.0°-60.0°W) to 32 m in the southern part (30.0°-32.5°N, 55.0°-65.0°W). The depth of one attenuation length at 490 nm is 1.2 to 1.9 times deeper than at 532 nm; the greatest differences occur to the south, and the least occur to the north. Finally, less spatial variability is exhibited than in the spring. The different spatial coverage also causes part of the difference. For example, the depth of four attenuation lengths varies spatially up to about 49 m at 490 nm and up to about 21 m at 532 nm.

The fall data, which come from 10.0°-40.0°N, 60.0°-79.0°W, span a wider range of latitudes than any of the data from the other seasons, but the range of longitudes is narrower. As seen in Figures 7 and 10 and Table 5, the diffuse attenuation at 490 nm is high in the region 35.0°-40.0°N, 70.0°-75.0°W (the depth of one attenuation length is 10 m), intermediate in the region 30.0°-35.0°N, 74.0°-79.0°W (the depth of one attenuation length is 16 m), and low in the region 10.0°-30.0°N, 60.0°-78.0°W (the depth of one attenuation length ranges from 21 to 26 m). Depths of 0.5 to 6.5 attenuation lengths at 490 nm are 1.7 times deeper than at 532 nm between

20.0° and 30.0°N, but the differences decrease to the south and to the north of that range of latitudes. Between 35.0° and 40.0°N, the depths of attenuation lengths are about the same at the two wavelengths down to four attenuation lengths. Diffuse attenuation at both wavelengths decreases from north (40.0°N) to south (20.0°N), but in the tropics (10.0°-20.0°N) the trend reverses. Between 20.0° and 40.0°N, considerable spatial variability is observed. For example, the depth of four attenuation lengths varies spatially up to 66 m at 490 nm and 25 m at 532 nm. At comparable latitudes (30.0°-40.0°N), the range in fall attenuation length profiles varies more than the summer and less than the spring data.

The main point of all these observations is that the attenuation of diffuse light varies considerably with location, wavelength, and depth. The geographic variations in these characteristics are briefly summarized as follows. At both 490 and 532 nm, the northwest Atlantic Ocean north of the Gulf Stream has large K_d values, and consequently the depth of the first attenuation length is only about 10 m or less. At 490 nm, the northeast Atlantic Ocean (28.0°-37.0°N, 14.5°-32.5°W), the Sargasso Sea, and the tropics have low K_d values, and the depth of the

Table 4. Summary of depths of attenuation lengths (in meters) in the Sargasso Sea in the summer.

No. of attenuation lengths	Depths of attenuation lengths (m) at various latitude (longitude) locations						
	30.0°-32.5°N (55.0°-65.0°W)	30.0°-35.0°N (50.0°-55.0°W)	32.5°-35.0°N (55.0°-65.0°W)	35.0°-40.0°N (50.0°-65.0°W)	40.0°-42.5°N (50.0°-65.0°W)	42.5°-45.0°N (50.0°-65.0°W)	45.0°-50.0°N (50.0°-60.0°W)
	Wavelength = 490 nm						
0.5	16.0	14.1	14.0	12.4	12.6	10.1	7.4
1.0	31.7	27.4	26.8	24.8	23.1	19.0	14.6
1.5	46.5	39.6	37.4	37.1	31.9	26.4	20.6
2.0	60.0	50.5	46.3	49.1	39.6	32.8	25.7
2.5	72.4	60.4	54.7	59.7	47.5	39.2	31.1
3.0	83.8	69.3	62.8	68.6	56.9	46.2	37.4
3.5	94.4	77.5	70.3	76.5	68.2	54.5	45.6
4.0	104.5	85.5	77.7	84.0	82.8	64.7	55.9
4.5	114.1	93.7	85.6	91.2	100.3	78.3	68.8
5.0	124.1	102.8	94.2	98.8	120.1	95.1	84.0
5.5	135.1	113.0	104.2	107.2	141.3	113.7	99.3
6.0	147.8	125.0	116.7	116.0	163.0	133.5	114.7
6.5	162.5	138.7	132.4	125.7	184.6	153.7	130.0
	Wavelength = 532 nm						
0.5	8.4	8.0	8.0	7.6	7.7	7.0	6.0
1.0	16.8	16.0	15.9	15.2	15.2	13.7	11.8
1.5	25.1	23.8	23.7	22.8	22.2	20.1	17.4
2.0	33.4	31.5	31.1	30.4	28.8	26.0	22.4
2.5	41.6	39.0	38.0	37.9	35.0	31.5	27.2
3.0	49.6	46.3	44.5	45.4	41.0	36.9	32.2
3.5	57.5	53.3	50.9	52.8	47.2	42.5	37.7
4.0	65.2	60.2	57.2	59.8	53.8	48.5	43.9
4.5	72.7	66.7	63.4	66.4	60.8	54.9	50.6
5.0	80.1	73.1	69.3	72.6	68.2	61.7	57.9
5.5	87.3	79.3	75.3	78.7	76.2	69.1	65.6
6.0	94.4	85.4	81.3	84.6	84.5	77.2	73.7
6.5	101.3	91.7	87.5	90.5	93.1	85.6	81.9

first attenuation length is about 20 m or greater. In these areas south of the Gulf Stream at 532 nm, the K_d values are intermediate, and the depth of the first attenuation length is 10 to 20 m. Therefore, the depths of the attenuation lengths at 532 nm are up to a factor of 2 shallower than at 490 nm. The attenuation of diffuse light also varies seasonally, but incomplete spatial coverage makes comparisons between seasons difficult. Much more data will be required to provide a complete picture of the seasonal and spatial variability of light attenuation across the North Atlantic Ocean.

REFERENCES

[1] Platt, P., and Sathyendranath, S., "Oceanic Primary Production: Estimation by Remote Sensing at Local and Regional Scales," *Science* **241**, 1613-1620 (1988).
[2] Kiefer, D.A., and Kremer, J. N., "Origins of Vertical Patterns of Phytoplankton and Nutrients in the Temperate, Open Ocean: A Stratigraphic Hypothesis," *Deep Sea Res.* **28A**, 1087-1105 (1981).
[3] Muller-Karger, F. E., Walsh, J. J., Evans, R.H., and Meyers, M.B., "On the Seasonal Phytoplankton Concentration and Sea Surface Temperature Cycles of the Gulf of Mexico as Determined by Satellites," *J. Geophys. Res.* **96**, 12,645-12,665 (1991).
[4] Taylor, A. H., Watson, A. J., Robertson, J. E., and Turner, D. R., "A Modeling Investigation of the Role of Phytoplankton in the Balance of Carbon at the Surface of the North Atlantic Ocean," *Global Biogeochem. Cycles* **5**, 151-171 (1991).
[5] Gordon, H.R., and Morel, A., *Remote Assessment of Ocean Color for Interpretation of Satellite Visible Imagery–A Review*, Springer-Verlag, New York (1983).
[6] Smith, R. C., and Baker, K. S., "The Bio-optical State of Ocean Waters and Remote Sensing," *Limnol. Oceanogr.* **23**, 247-259 (1978).
[7] Baker, K. S., and Smith, R. C., "Bio-optical Classification and Model of Natural Waters. 2," *Limnol. Oceanogr.* **27**, 500-509 (1982).
[8] Winn, C. W., Chiswell, S., Firing, E., Karl, D., and Lucas, R., *Hawaii Ocean Time-Series Program Data Report 2 1990*, School of Ocean and Earth Science and Technology, University of Hawaii, Report SOEST-92-1 (December 1991).
[9] Stark, V. L., *Optical Attenuation in the Northeast Pacific Ocean*, JHU/APL STD-N-423 (May 1986).
[10] Morel, A., and Berthon, J., "Surface Pigments, Algal Biomass Profiles, and Potential Production of the Euphotic Layer: Relationships Reinvestigated in View of Remote-Sensing Applications," *Limnol. Oceanogr.* **34**, 1545-1562 (1989).
[11] Baker, K. S., and Smith, R. C., "Quasi-Inherent Characteristics of the Diffuse Attenuation Coefficient for Irradiance," *Proc. SPIE* **208**, 60-62 (1979).
[12] Kirk, J. T. O., "Dependence of Relationship Between Inherent and Apparent Optical Properties of Water on Solar Altitude," *Limnol. Oceanogr.* **29**, 350-356 (1984).

Table 5. Summary of depths of attenuation lengths (in meters) in the Sargasso Sea in the fall.

No. of attenuation lengths	Depths of attenuation lengths (m) at various latitude (longitude) locations			
	10.0°–20.0°N (60.0°–65.0°W)	20.0°–30.0°N (68.0°–78.0°W)	30.0°–35.0°N (74.0°–79.0°W)	35.0°–40.0°N (70.0°–75.0°W)
Wavelength = 490 nm				
0.5	10.2	12.8	7.8	4.8
1.0	20.7	25.6	15.6	9.6
1.5	31.2	38.5	23.5	14.1
2.0	41.4	51.5	31.4	18.6
2.5	51.3	64.4	39.3	23.1
3.0	60.8	77.5	47.2	27.9
3.5	70.0	90.8	55.2	32.8
4.0	79.1	104.1	63.4	38.1
4.5	88.4	117.8	72.2	43.8
5.0	98.2	131.6	81.2	49.9
5.5	109.6	145.4	90.6	56.3
6.0	123.6	159.3	100.8	62.9
6.5	139.7	173.1	111.6	70.1
Wavelength = 532 nm				
0.5	7.0	7.7	6.1	4.6
1.0	14.0	15.4	12.2	9.1
1.5	21.1	23.1	18.3	13.6
2.0	28.1	30.8	24.4	17.9
2.5	35.1	38.5	30.6	22.3
3.0	42.1	46.3	36.7	26.8
3.5	49.0	54.0	42.8	31.5
4.0	55.8	61.7	49.0	36.3
4.5	62.4	69.5	55.2	41.3
5.0	69.1	77.2	61.4	46.5
5.5	75.7	85.0	67.8	51.9
6.0	82.3	92.9	74.4	57.4
6.5	89.0	100.7	81.0	63.0

[13] Austin, R., and Petzold, T., "Spectral Dependence of the Diffuse Attenuation Coefficient of Light in Ocean Waters," *Opt. Eng.* **25**, 471-479 (1986).

[14] Austin, R., and Petzold, T. "Spectral Dependence of the Diffuse Attenuation Coefficient of Light in Ocean Waters: A Re-examination Using New Data," *Proc. SPIE* **1302**, 79-93 (1990).

[15] Smart, J. H., *Atlas of Optical Profiles in the Atlantic and Pacific Oceans and in Selected Coastal Areas*, JHU/APL STD-R-2149 (Oct 1992).

[16] Stark, V. L., *Variability of Reflectance as Inferred from CZCS Data*, JHU/APL STD-R-2029 (Oct 1991).

[17] Parsons, T. R., Takahashi, M., and Hargrave, B., *Biological Oceanographic Processes*, Third Edition, Pergamon Press, Oxford, England, pp. 24-28 (1984).

[18] Sinex, C. H., *A Simple Model for the Occurrence of the Spring Bloom*, JHU/APL STD-N-313 (Jan 1985).

[19] Marshall, B. R., and Smith, R. C., "Raman Scattering and In-Water Ocean Optical Properties," *Appl. Opt.* **29**, 71-84 (1990).

[20] Stavn, R. H., and Weidemann, A. D., "Optical Modeling of Clear Ocean Light Fields: Raman Scattering Effects," *Appl. Opt.* **27**, 4002-4011 (1988).

[21] Cowles, T. J., "In Situ Monitoring of Ocean Chlorophyll via Laser-Induced Fluorescence Backscattering Through an Optical Fiber," *Appl. Opt.* **28**, 595-600 (1989).

[22] Stavn, R. H., and Weidemann, A. D., "Raman Scattering Effects in Ocean Optics," *Proc. SPIE* **925**, 131-139 (1988).

[23] Stavn, R. H., and Weidemann, A. D., "Raman Scattering Effects at the Shorter Visible Wavelengths in Clear Ocean Waters," *Proc. SPIE* **1302**, 94-99 (1990).

[24] Siegel, D. A., and Dickey, T. D., "Observations of the Vertical Structure of the Diffuse Attenuation Spectrum," *Deep Sea Res.* **34**, 547-563 (1987).

THE AUTHOR
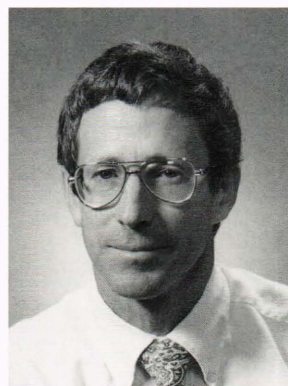
JEFFREY H. SMART received a B.S. in physics in 1975 from Oakland University and an M.S. in atomic physics in 1977 from Wayne State University. From 1978 to 1984, he served as an Associate Physicist in the Environment Investigations Group of the APL Submarine Technology Department, developing an ocean shear instrument system and its in-house analysis program. Since 1984, Mr. Smart has served as a senior physicist at APL, and has become a recognized expert in the analysis of ocean current data. He has also served as the lead project environmental specialist on numerous U.S. Navy projects. He is currently specializing in ocean measurements and analysis of basic optical properties such as scattering and absorption of light. In 1993, as a result of his fifteen years of experience in the ocean environment, he was given the honor of serving on the Naval Review Board at the National Academy of Sciences. He is a member of the American Geophysical Union and the IEEE.